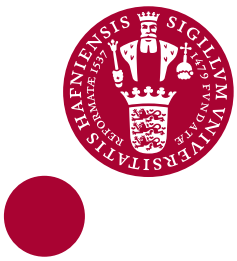

SIRT7-Dependent Deacetylation of Fibrillarin Controls Histone H2A Methylation and rRNA Synthesis during the Cell Cycle

Iyer-Bierhoff, Aishwarya; Krogh, Nicolai; Tessarz, Peter; Ruppert, Thomas; Nielsen, Henrik; Grummt, Ingrid

Published in:
Cell Reports

DOI:
10.1016/j.celrep.2018.11.051

Publication date:
2018

Document version
Publisher's PDF, also known as Version of record

Report

Cell Reports

SIRT7-Dependent Deacetylation of Fibrillarin Controls Histone H2A Methylation and rRNA Synthesis during the Cell Cycle

Graphical Abstract

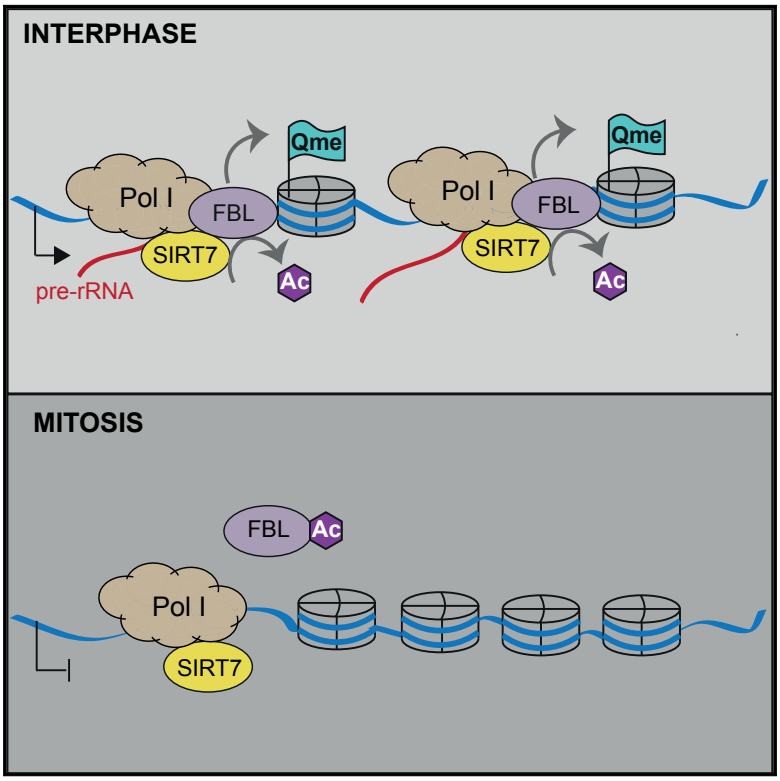

Authors

Aishwarya Iyer-Bierhoff, Nicolai Krogh, Peter Tessarz, Thomas Ruppert, Henrik Nielsen, Ingrid Grummt

Correspondence

i.grummt@dkfz.de

In Brief

Iyer-Bierhoff et al. show that reversible acetylation of fibrillarin (FBL) regulates methylation of histone H2A at glutamine 104 (H2AQ104) and controls rDNA transcription. The study identifies a mechanism underlying cell-cycle-dependent fluctuations in H2AQ104 methylation and rRNA synthesis driven by SIRT7-mediated deacetylation of FBL.

Highlights

- FBL is acetylated by CBP and deacetylated by the NAD^+-dependent deacetylase SIRT7
- Acetylation of FBL does not affect rRNA methylation and processing
- Acetylation compromises FBL-dependent methylation of H2AQ104
- FBL acetylation and loss of H2AQ104me regulate mitotic repression of rDNA transcription

Iyer-Bierhoff et al., 2018, Cell Reports *25*, 2946–2954
December 11, 2018
https://doi.org/10.1016/j.celrep.2018.11.051

CellPress

OPEN ACCESS
CellPress

Cell Reports
Report

SIRT7-Dependent Deacetylation of Fibrillarin Controls Histone H2A Methylation and rRNA Synthesis during the Cell Cycle

Aishwarya Iyer-Bierhoff,[1] Nicolai Krogh,[2] Peter Tessarz,[3] Thomas Ruppert,[4] Henrik Nielsen,[2] and Ingrid Grummt[1,5,*]
[1]Molecular Biology of the Cell II, German Cancer Research Centre (DKFZ), DKFZ-Zentrum für Molekulare Biologie der Universität Heidelberg (ZMBH) Alliance, 69120 Heidelberg, Germany
[2]Department of Cellular and Molecular Medicine, University of Copenhagen, 2200N Copenhagen, Denmark
[3]Department of Chromatin and Ageing, Max Planck Institute for Biology of Ageing, 50931 Cologne, Germany
[4]Center for Molecular Biology of Heidelberg University (ZMBH), DKFZ-ZMBH Alliance, 69120 Heidelberg, Germany
[5]Lead Contact
*Correspondence: i.grummt@dkfz.de
https://doi.org/10.1016/j.celrep.2018.11.051

SUMMARY

Fibrillarin (FBL) is a dual-function nucleolar protein that catalyzes 2′-*O* methylation of pre-rRNA and methylation of histone H2A at glutamine 104 (H2AQ104me). The mechanisms that regulate FBL activity are unexplored. Here, we show that FBL is acetylated at several lysine residues by the acetyltransferase CBP and deacetylated by SIRT7. While reversible acetylation does not impact FBL-mediated pre-rRNA methylation, hyperacetylation impairs the interaction of FBL with histone H2A and chromatin, thereby compromising H2AQ104 methylation (H2AQ104me) and rDNA transcription. SIRT7-dependent deacetylation of FBL ensures H2AQ104me and high levels of rRNA synthesis during interphase. At the onset of mitosis, nucleolar disassembly is accompanied by hyperacetylation of FBL, loss of H2AQ104me, and repression of polymerase I (Pol I) transcription. Overexpression of an acetylation-deficient, but not an acetylation-mimicking, FBL mutant restores H2AQ104me and transcriptional activity. The results reveal that SIRT7-dependent deacetylation impacts nucleolar activity by an FBL-driven circuitry that mediates cell-cycle-dependent fluctuation of rDNA transcription.

INTRODUCTION

Acetylation of histones and regulatory proteins by lysine acetyltransferases (KATs) plays major roles in the regulation of gene expression by linking cell signaling pathways to chromatin structure and transcriptional activity. Like many other protein modifications, acetylation is reversible. Mammalian lysine deacetylases (KDACs) are classified into three subgroups based on sequence similarity and cofactor requirement. Class III KDACs, the sirtuin family of protein deacetylases, require the cofactor NAD^+ for lysine deacetylation. The seven mammalian sirtuins, denoted SIRT1–SIRT7, have distinct cellular localizations and target multiple substrates (Michishita et al., 2005). The nucleolar member of the sirtuin family, SIRT7, stimulates transcription of rRNA genes (rDNA) and ribosome biogenesis (Chen et al., 2013; Ford et al., 2006). Previous work has established that SIRT7 activates rDNA transcription by deacetylating polymerase-associated factor 53 (PAF53), a subunit of mammalian RNA polymerase I (Pol I) (Chen et al., 2013). SIRT7 also regulates pre-rRNA processing by deacetylating U3-55k, a core component of the U3 small nucleolar ribonucleoprotein (snoRNP) complex (Chen et al., 2016). The role of SIRT7 in ribosome biogenesis and cell proliferation is also supported by recent proteomic analyses showing that SIRT7 is associated with numerous proteins that are involved in transcription, ribosome biogenesis, and translation (Tsai et al., 2014; Blank et al., 2017). Among SIRT7-associated proteins was fibrillarin (FBL), a conserved nucleolar protein that is required for 2′-*O*-methylation of pre-rRNA, early cleavage steps, and ribosome assembly (Tollervey et al., 1991, 1993; Tyc and Steitz, 1989). FBL is a component of snoRNPs containing NOP56, NOP58, NHP2L1, and box C/D small nucleolar RNAs (snoRNAs) that guide FBL to specific positions in rRNA. Some sites in rRNA are differentially methylated, which may account for ribosome heterogeneity under certain physiological conditions (Birkedal et al., 2015; Krogh et al., 2016).

In addition to methylation of rRNA, FBL was found to methylate histone H2A at glutamine (Q) 104 in mammals, Q105 in yeast, and Q106 in plants (Loza-Muller et al., 2015; Tessarz et al., 2014). Glutamine methylation of histone H2A positively correlates with Pol I transcription. How H2AQ104 methylation is regulated, affects chromatin architecture, and is linked to rDNA transcription is not known. FBL is acetylated at several lysine residues (Choudhary et al., 2009; Schölz et al., 2015), suggesting that reversible acetylation regulates FBL activity. Here, we show that FBL acetylation does not affect rRNA methylation and pre-rRNA processing but attenuates FBL binding to histone H2A and compromises Q104 methylation. Conversely, deacetylation by SIRT7 increases H2AQ104 methylation (H2AQ104me) and enhances Pol I transcription. Acetylation-dependent regulation of FBL activity links cell-cycle-dependent fluctuations of Pol I transcription to H2AQ104me levels. At the onset of mitosis,

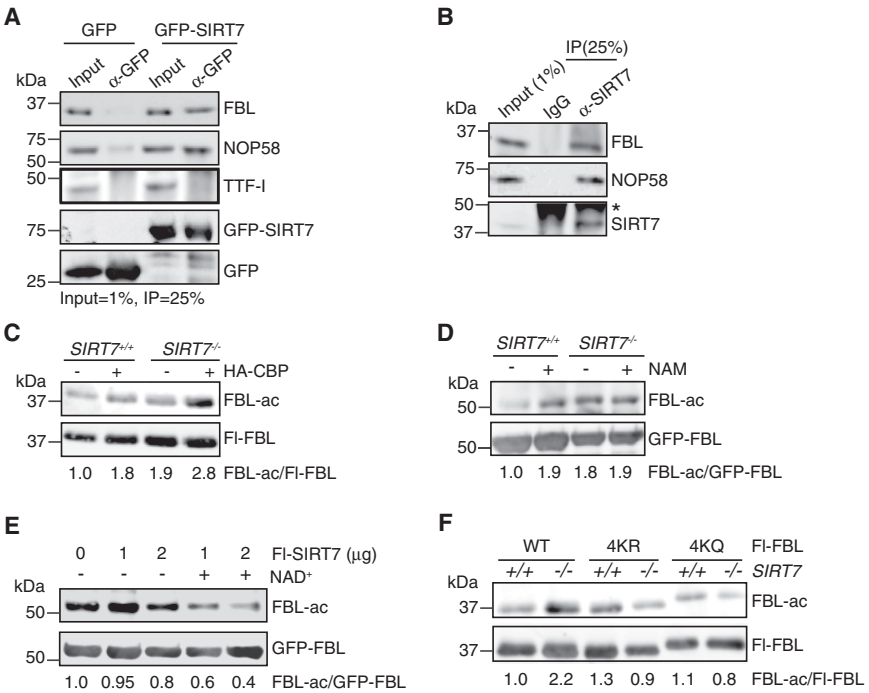

Figure 1. SIRT7 Deacetylates FBL

(A) Immunoblots showing co-immunoprecipitation of GFP-SIRT7 with FBL, NOP58, and TTF-I.

(B) Immunoblots showing co-immunoprecipitation of endogenous SIRT7 with FBL and NOP58. Asterisk indicates a heavy-chain immunoglobulin G (IgG) band that migrates at ~50 kDa.

(C) Western blot with pan-ac-K antibody showing acetylation of Fl-FBL expressed in *SIRT7*$^{+/+}$ and *SIRT7*$^{-/-}$ HEK293T cells in the absence or presence of hemagglutinin (HA)-tagged CBP.

(D) Acetylation of GFP-FBL from *SIRT7*$^{+/+}$ and *SIRT7*$^{-/-}$ cells with or without NAM treatment (10 mM, 5 hr).

(E) *In vitro* deacetylation assay of GFP-FBL from *SIRT7*$^{-/-}$ HEK293T cells using purified Fl-SIRT7.

(F) Western blot monitoring acetylation of wild-type (WT) and mutant (4KR and 4KQ) FBL expressed in *SIRT7*$^{+/+}$ or *SIRT7*$^{-/-}$ cells. Note that 4KQ-FBL migrates slower than WT and 4KR-FBL. FBL-ac/tagged FBL represents the ratio of acetylated to total immunoprecipitated FBL normalized to control (lane 1).

See also Figure S1.

FBL is released from the nucleolus organizer regions (NORs) and is distributed to the perichromosomal region (Dundr et al., 2000). This relocalization prevents the interaction with SIRT7, which leads to hyperacetylation of FBL, loss of H2AQ104me, and establishment of a transcription-refractive chromatin structure. At the exit from mitosis, deacetylation of FBL facilitates restoration of H2AQ104me and resumption of rDNA transcription. The results provide insights into the control of nucleolar activity by a SIRT7- and FBL-driven circuitry that impacts H2AQ104 methylation and rDNA transcription.

RESULTS

SIRT7 Deacetylates FBL

To validate the association of SIRT7 with box C/D snoRNPs, we monitored the interaction of SIRT7 with FBL and NOP58 by co-immunoprecipitation experiments. Consistent with mass spectrometric data showing that SIRT7 interacts with box C/D snoRNP components (Blank et al., 2017; Tsai et al., 2014), these experiments revealed the association of SIRT7 with FBL and NOP58, but not with the Pol I-specific transcription termination factor TTF-I (Figures 1A, 1B, and S1A).

Previous acetylome analyses revealed that FBL is acetylated at multiple lysine residues (Choudhary et al., 2009; Schölz et al., 2015). To identify the acetyltransferases that acetylate FBL, we co-expressed GFP-tagged FBL with p300, CBP, or PCAF and examined the acetylation state of GFP-FBL on western blots with an antibody that recognizes acetyl-lysine (ac-K). While acetylation was hardly detectable in untransfected cells and cells overexpressing p300 or PCAF, there was a clear signal after overexpression of CBP (Figure S1B). In support of SIRT7 counteracting CBP-mediated acetylation of FBL, acetylation increased 2-fold in the presence of nicotinamide (NAM), a specific inhibitor of NAD^+-dependent sirtuins, whereas treatment with trichostatin A (TSA), an inhibitor of class I and II deacetylases, did not alter FBL acetylation (Figure S1C).

To examine whether SIRT7 reverts CBP-mediated acetylation of FBL, we compared the acetylation state of FBL isolated from parental HEK293T cells (*SIRT7*$^{+/+}$) and *SIRT7*$^{-/-}$ cells in which both *SIRT7* alleles were inactivated by CRISPR (clustered regularly interspaced short palindromic repeats)/Cas9-mediated mutagenesis (Chen et al., 2016). In support of SIRT7 targeting FBL, acetylation of FBL was higher in *SIRT7*$^{-/-}$ cells than *SIRT7*$^{+/+}$ cells and was further augmented by overexpression of CBP (Figure 1C). Conversely, overexpression of GFP-SIRT7 decreased FBL acetylation in *SIRT7*$^{-/-}$ cells. (Figure S1D). FBL acetylation in *SIRT7*$^{-/-}$ cells was not further augmented by treatment with NAM, indicating that SIRT7 is the major (if not only) sirtuin that targets FBL (Figure 1D).

To demonstrate that SIRT7 deacetylates FBL, we performed *in vitro* deacetylation assays using hyperacetylated GFP-FBL from *SIRT7*$^{-/-}$ cells. Acetylation of GFP-FBL was markedly decreased in the presence of immunopurified SIRT7 and NAD^+, confirming that FBL is deacetylated by SIRT7 (Figure 1E).

Global acetylome studies have shown that FBL is acetylated at four conserved lysine residues (K102, K121, K205, and K206) (Choudhary et al., 2009; Schölz et al., 2015) (Figure S1E). To examine whether SIRT7 targets these lysine residues, we replaced them by either arginine (4KR) or glutamine (4KQ) to mimic the hypo- or hyperacetylated state of FBL, respectively. While acetylation of wild-type (WT) FBL was 2.4-fold higher in *SIRT7*$^{-/-}$ cells than *SIRT7*$^{+/+}$ cells, acetylation of the 4KR- or 4KQ-FBL mutants did not increase, substantiating that the mutated lysines are targeted by SIRT7 (Figure 1F).

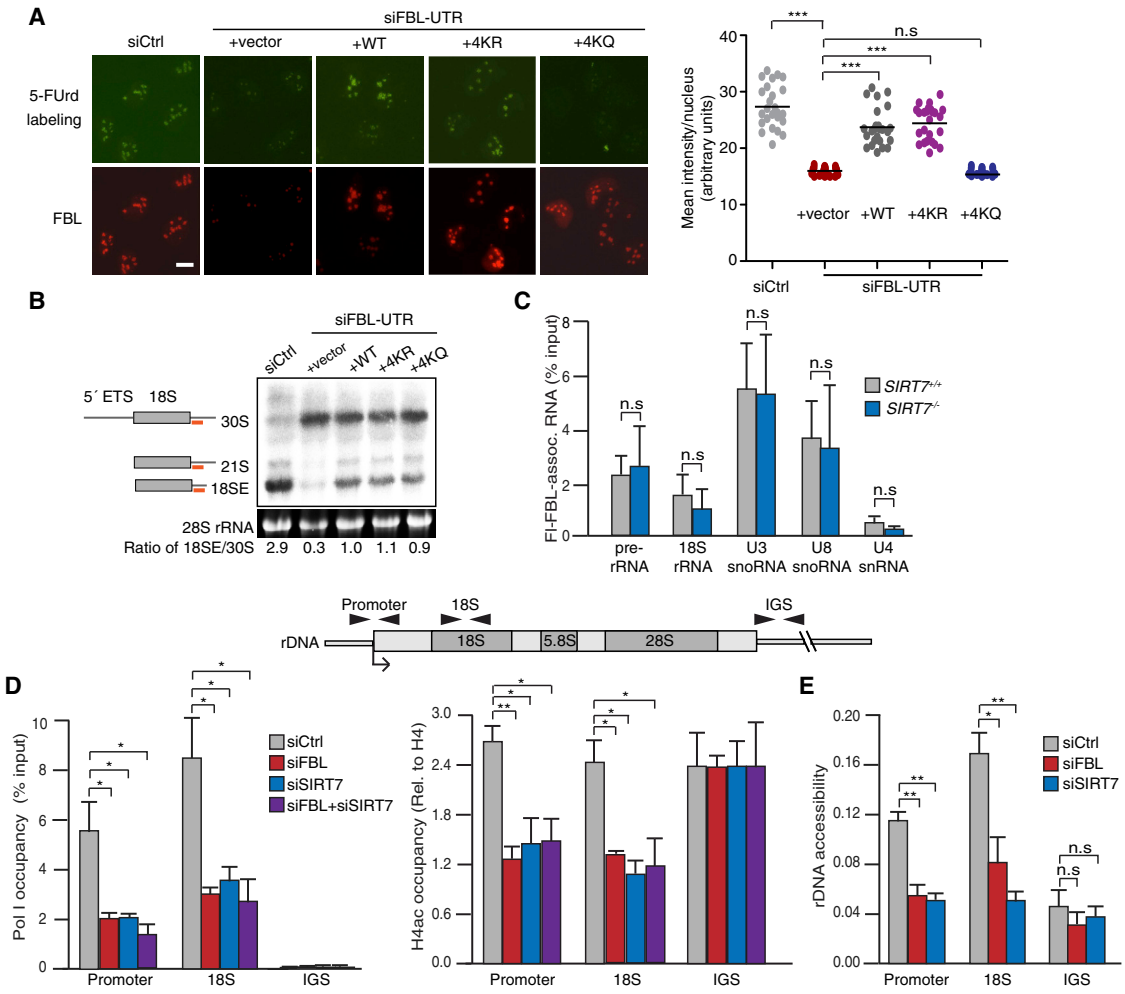

Figure 2. FBL Acetylation Inhibits Pre-rRNA Synthesis, but Not Methylation and Processing

(A) Immunostaining of 5-FUrd-labeled RNA in FBL-depleted U2OS cells expressing FLAG-tagged WT-, 4KR-, or 4KQ-FBL. Labeled RNA is stained with anti-BrdU (green) and FBL (red). Scale bar, 10 μm. Quantification shows 5-FUrd staining as mean intensity per nucleus (n = 30–40 cells from three biological replicates). Unpaired t test with Welch's correction was applied. ***$p \leq 0.001$. See also Figure S2A.

(B) Northern blot of RNA from U2OS cells expressing WT or mutant FBL. The scheme on the left indicates rRNA processing intermediates hybridizing to the radiolabeled ITS1 probe (orange). The ratio of 18SE to 30S rRNA is shown below. See also Figure S2A.

(C) CLIP-qRT-PCR monitoring pre-rRNA and snoRNA binding of FI-FBL in *SIRT7*$^{+/+}$ and *SIRT7*$^{-/-}$ cells.

(D) ChIP-qPCR showing rDNA occupancy of Pol I and acetylated histone H4 (H4ac) in HEK293T cells transfected with control siRNAs or siRNAs targeting FBL, SIRT7, or both. Data are shown as percentage of input, and H4ac is normalized to total histone H4. The position of amplicons is shown. See also Figures S2F and S2G.

(E) FAIRE-qPCR showing chromatin accessibility of rDNA in control, FBL-, and SIRT7-depleted HEK293T cells. Data represent the ratio of extracted chromatin to input.

Bars represent mean ± SEM; n = 3. *$p \leq 0.05$, **$p \leq 0.01$, n.s, nonsignificant.

See also Figure S2 and Table S2.

FBL Acetylation Inhibits Pre-rRNA Synthesis, but Not Methylation or Processing

To study the impact of FBL acetylation on pre-rRNA synthesis and maturation, we depleted cells of FBL using small interfering RNA (siRNA) that targets the 3′ UTR of *FBL* mRNA and assayed nucleolar transcription after overexpression of wild-type and mutant FBL. After pulse-labeling with 5-fluorouridine (5-FUrd) and immunostaining with anti-bromodeoxyuridine (anti-BrdU) antibody, bright nucleolar signals were observed in control cells. There was hardly any nucleolar staining in FBL knockdown cells. Overexpression of wild-type FBL or the acetylation-deficient 4KR mutant, but not the acetylation-mimetic 4KQ mutant, restored pre-rRNA synthesis (Figures 2A and S2A). Overexpression of single or double K→Q mutants rescued transcription similar to WT-FBL (Figure S2B). Recent mass spectrometric analysis revealed that K102, K121, and K205 are hyperacetylated in SIRT7-deficient cells, substantiating that SIRT7 targets several lysines in FBL.

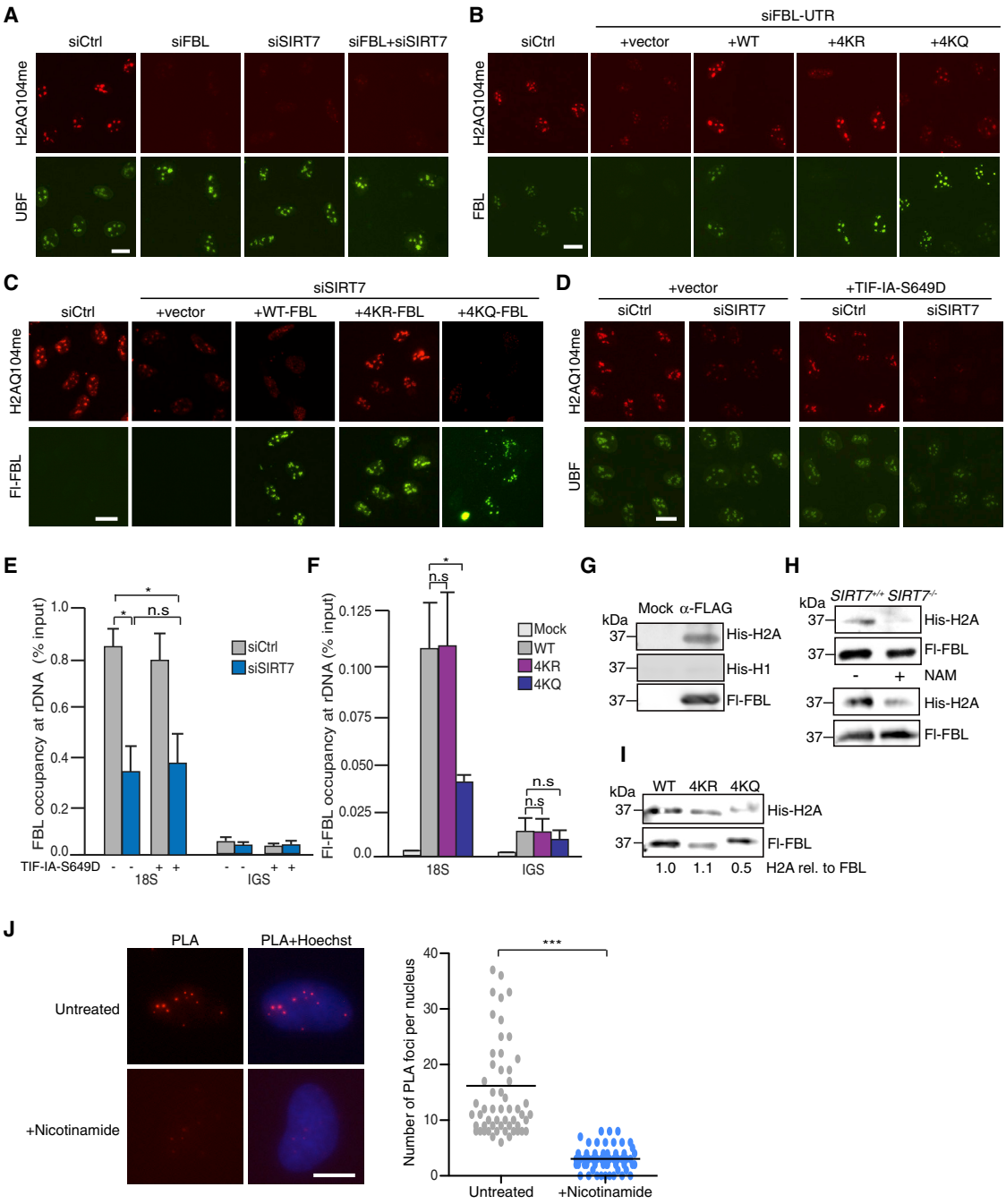

Figure 3. Acetylation of FBL Regulates Glutamine Methylation

(A) U2OS cells transfected with control siRNA or siRNAs against FBL or SIRT7 or both, were stained with antibodies against H2AQ104me (red) and UBF (green). Scale bar, 10 μm.

(B) U2OS cells depleted of FBL by 3′ UTR-targeting siRNA were transfected with plasmids encoding wild-type or mutant FBL. Cells were stained with anti-H2AQ104me (red) and anti-FBL (green) antibodies. Scale bar, 10 μm. See Figure S3E for quantification.

(C) H2AQ104 methylation in control or SIRT7-depleted U2OS cells overexpressing FLAG-tagged WT-, 4KR-, or 4KQ-FBL. Cells were stained with anti-H2AQ104me (red) and anti-FLAG antibodies (green). Scale bar, 10 μm. See also Figure S3F.

(D) H2AQ104me in control or SIRT7-depleted U2OS cells overexpressing TIF-IA-S649D. Cells were stained with anti-H2AQ104me (red) and anti-UBF (green) antibodies. Scale bar, 10 μm. See also Figures S3G–S3I.

(E) ChIP-qPCR showing rDNA occupancy of FBL in control and SIRT7-depleted cells expressing Fl-TIF-IA-S649D. Percentage of input after subtraction of IgG values is shown.

(F) qPCR showing rDNA occupancy of anti-FLAG ChIPs from mock-transfected HEK293T cells or cells expressing WT-, 4KR-, or 4KQ-FBL. Percentage of input after subtraction of IgG values is shown. See also Figure S3J.

(legend continued on next page)

To investigate the molecular mechanism by which acetylation of FBL impairs Pol I transcription, we first examined whether acetylation affects pre-rRNA processing. Northern blot analysis using an ITS1 probe that detects rRNA processing intermediates revealed accumulation of 30S rRNA at the expense of 21S and 18SE rRNA in FBL-deficient cells (Figure 2B). Both wild-type FBL and the two mutants partially rescued the processing defect, as seen by increased levels of 21S and 18SE processing intermediates compared to FBL-depleted cells, indicating that the acetylation state of FBL does not affect pre-rRNA processing. Moreover, cross-linking immunoprecipitation (CLIP) experiments revealed that hyperacetylated FBL from *SIRT7*$^{-/-}$ cells bound to rRNA and snoRNAs similarly as FBL from parental *SIRT7*$^{+/+}$ cells (Figure 2C). Thus, acetylation affects neither pre-rRNA processing nor the interaction of FBL with RNA.

Given that FBL exerts a key function in 2′-*O* ribose methylation (Kiss-László et al., 1996), we reasoned that acetylation might regulate rRNA methylation. To test this, we subjected RNA from *SIRT7*$^{+/+}$ and *SIRT7*$^{-/-}$ HEK293T cells to RiboMeth-seq, a quantitative high-throughput method that interrogates RNA ribose methylation based on protection from alkaline cleavage by the 2′-*O*-methyl (2′-*O*-Me) group (Birkedal et al., 2015). RiboMeth-seq profiles of RNA from *SIRT7*$^{+/+}$ and *SIRT7*$^{-/-}$ cells revealed only two minor differences in cytoplasmic RNA (Figure S2C) and no differences in nuclear RNA (Figure S2D). Depletion of SIRT7 by siRNAs also did not affect 2′-*O*-Me (Figure S2E), indicating that FBL acetylation does not impact rRNA methylation.

Knockdown of FBL, SIRT7, or both proteins decreased Pol I occupancy at rDNA, while the association of UBF with rDNA remained unaffected. The level of acetylated histone H4 (H4ac) was also reduced, suggesting that FBL and SIRT7 contribute to the establishment of a transcription-permissive chromatin structure (Figures 2D, S2F, and S2G). This view is supported by formaldehyde-assisted isolation of regulatory elements (FAIRE) assays, which measure nucleosome density according to chromatin extractability. Consistent with SIRT7-mediated deacetylation of FBL being conducive to transcription, the fraction of extractable rDNA was significantly reduced in both FBL- and SIRT7-depleted cells (Figure 2E). The intriguing correlations among hypoacetylation of FBL, chromatin opening, Pol I recruitment and rDNA transcription suggest that the acetylation state of FBL plays a key role in chromatin-based processes that promote Pol I transcription.

Acetylation Impairs the Interaction of FBL with Histone H2A and Attenuates Glutamine Methylation

In addition to its established function in pre-rRNA methylation, FBL is known to methylate nucleolar histone H2A at glutamine 104 (Tessarz et al., 2014). As acetylation of FBL impaired Pol I transcription without affecting pre-rRNA processing and RNA methylation, we reasoned that acetylation might regulate FBL-directed histone methylation. Current batches of anti-H2AQ104me antibody yield high background in chromatin immunoprecipitations (ChIPs) and western blots but reliably stain nucleolar H2AQ104me. We therefore monitored the link between FBL acetylation and H2AQ104 methylation by quantitative immunofluorescence. In accord with a previous study (Tessarz et al., 2014), nucleolar staining of H2AQ104me was abolished after knockdown of FBL. Knockdown of SIRT7 or double knockdown of SIRT7 and FBL led to similar reduction in H2AQ104me, indicating that SIRT7-mediated deacetylation of FBL promotes H2AQ104 methylation (Figure 3A). Inhibition of H2AQ104me and pre-rRNA synthesis in SIRT7-depleted cells was overcome by expression of wild-type SIRT7, but not a catalytically inactive SIRT7 mutant (SIRT7-H187Y), demonstrating that the enzymatic activity of SIRT7 is required for H2A methylation and rDNA transcription (Figures S3A–S3C). Inhibition of SIRT7 by nicotinamide or overexpression of CBP attenuated the H2AQ104me signal, reinforcing that hyperacetylation of FBL impairs H2AQ104 methylation (Figure S3D).

To validate the relevance of FBL acetylation in H2AQ104 methylation, we examined H2AQ104me after overexpression of wild-type or mutant FBL in FBL-deficient cells. In accord with FBL being required for H2AQ104me, knockdown of FBL abolished H2AQ104me. While wild-type FBL and the 4KR mutant rescued H2AQ104me, the 4KQ mutant did not promote H2AQ104me (Figures 3B and S3E). Strikingly, H2AQ104me was also attenuated by depletion of SIRT7. As in FBL-deficient cells, H2AQ104me was rescued by 4KR-FBL, but not 4KQ-FBL or wild-type FBL, which is hyperacetylated in SIRT7-deficient cells (Figures 3C and S3F). Together, these results reveal that SIRT7-mediated deacetylation of FBL is required for H2AQ104 methylation.

To exclude that the decreased level of H2AQ104me is due to secondary effects brought about by diminished pre-rRNA synthesis in SIRT7-depleted cells, we monitored H2AQ104me after augmenting Pol I transcription by overexpression of TIF-IA-S649D, a constitutively active mutant of the Pol-I-specific transcription initiation factor TIF-IA (Zhao et al., 2003). TIF-IA-S649D enhanced rDNA transcription and Pol I binding in control cells and also restored nucleolar transcription in SIRT7-depleted cells (Figures S3G–S3I). H2AQ104me, however, remained low in SIRT7-depleted cells, regardless whether or not Pol I transcription was activated by TIF-IA-S649D (Figure 3D). Thus, increased Pol I transcription alone is not sufficient to foster H2AQ104me but requires deacetylation of FBL by SIRT7. The association of FBL with rDNA was reduced in SIRT7-depleted cells, regardless whether or not TIF-IA-S649D was overexpressed (Figure 3E). Wild-type and the 4KR-FBL mutant efficiently bound to rDNA, whereas binding of the acetylation-mimetic 4KQ-FBL mutant

(G) Far-western blots with anti-His and anti-FLAG antibodies showing binding of His-tagged histones H2A and H1 to Fl-FBL. See also Figure S3K.
(H) Far-western blot showing binding of His-H2A to Fl-FBL immunopurified from *SIRT7*$^{+/+}$, *SIRT7*$^{-/-}$ (top) or NAM-treated (bottom) HEK293T cells.
(I) Far-western blot showing binding of WT and mutant FBL to His-H2A. The ratio of H2A to FBL is normalized to WT (lane 1).
(J) Untreated or NAM-treated U2OS cells were subjected to PLA with anti-FBL and anti-H2A antibodies. PLA signals are visualized as red foci and nuclei by Hoechst 33342 staining. Quantification shows number of PLA foci per nucleus (n = 50–60 cells from three biological replicates). Unpaired t test with Welch's correction was applied. ***$p \leq 0.001$. Scale bar, 10 μm. See also Figure S3M.
Bars represent mean ± SEM; n = 3. *$p \leq 0.05$, **$p \leq 0.01$.

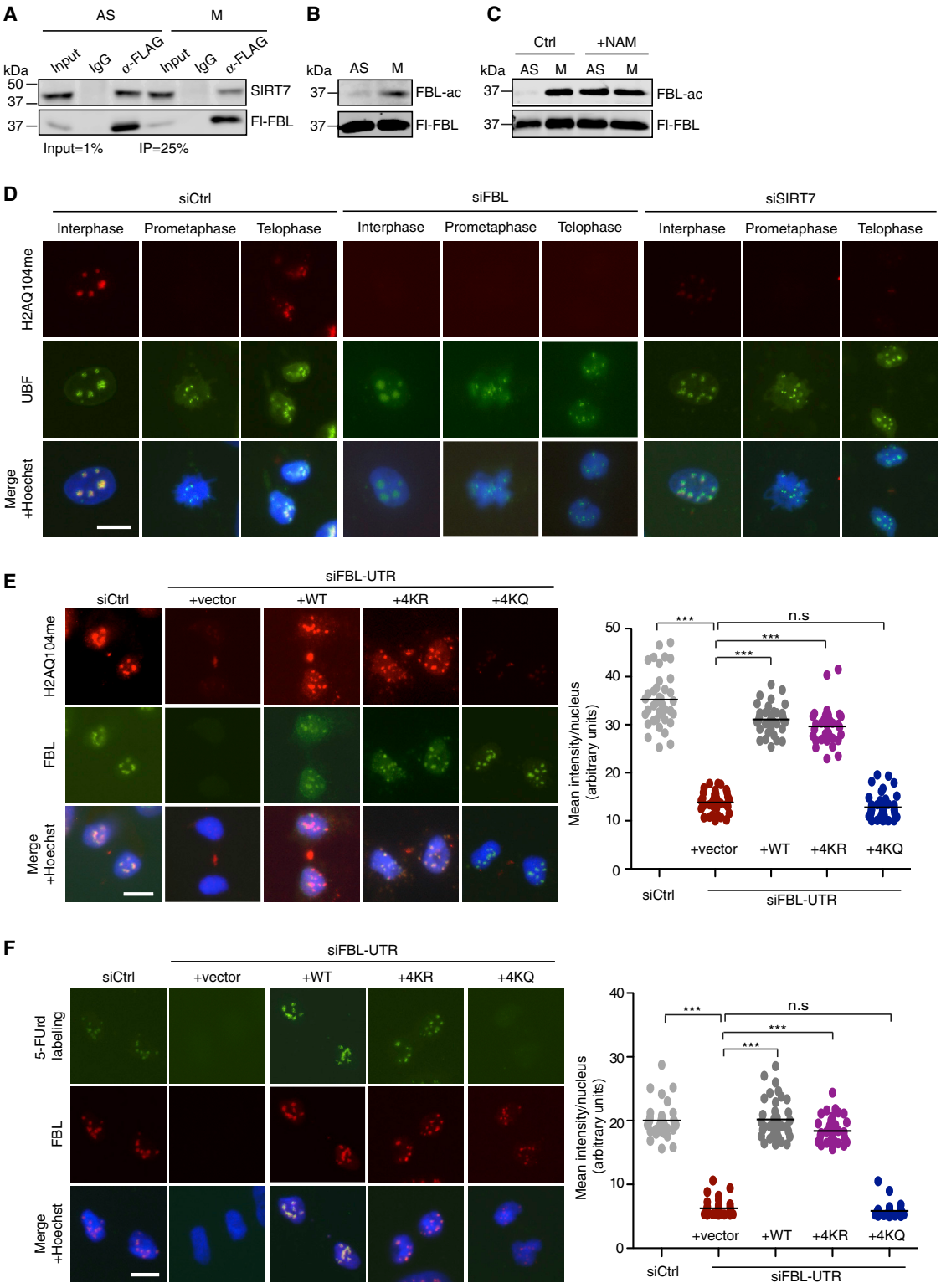

Figure 4. Hyperacetylation of FBL Attenuates H2AQ104me and rDNA Transcription during Mitosis

(A) Immunoblot showing co-immunoprecipitation of Fl-FBL and SIRT7 in asynchronous (AS) and nocodazole-arrested (100 ng/mL, 16 hr) mitotic (M) HEK293T cells. See also Figure S4A.

(B) Acetylation of Fl-FBL from asynchronous (AS) or mitotic (M) HEK293T cells was monitored on immunoblots with anti-pan-ac-K antibody. See also Figure S4A.

(legend continued on next page)

was significantly lower (Figures 3F and S3J). These results imply that acetylation impairs binding of FBL to rDNA, which in turn attenuates H2AQ104me.

To examine whether reversible acetylation regulates binding of FBL to histone H2A, we monitored the interaction of FBL with histones by Far-western blot assays. Immunopurified FBL was subjected to gel electrophoresis and transferred to a nitrocellulose membrane, and binding of His-tagged H2A and H1 was visualized on western blots. This assay revealed that FBL directly and specifically interacts with histone H2A (Figures 3G and S3K). Binding to histone H2A was compromised if FBL was purified from *SIRT7*$^{-/-}$ cells or from cells treated with NAM (Figure 3H). Accordingly, wild-type FBL and the 4KR mutant bound H2A more efficiently than 4KQ-FBL, corroborating that hypoacetylation promotes the interaction of FBL with H2A (Figure 3I). In a complementary approach, we used immobilized His-tagged histone H2A to pull down FBL from nuclear lysates. FBL from control cells was efficiently pulled down by histone H2A. Inhibition of SIRT7 with nicotinamide decreased the FBL-H2A interaction, underscoring the impact of SIRT7 activity on the association of FBL with H2A (Figure S3L).

To examine the association of endogenous FBL with histone H2A *in vivo*, we performed proximity ligation assays (PLA) using anti-FBL and anti-H2A antibodies. Several bright nuclear foci were visible in unperturbed cells, demonstrating the close proximity (<40 nm) of FBL and histone H2A. Treatment with nicotinamide markedly reduced the PLA signal, supporting that acetylation impairs the interaction of FBL with H2A (Figures 3J and S3M). While acetylation did not affect FBL binding to NOP58 or snoRNAs (Figures S3N and 2C), knockdown of NOP58 led to decreased levels of FBL, compromised rDNA transcription, and diminished H2AQ104me (Figures S3O and S3P).

Hyperacetylation of FBL Attenuates H2AQ104me and rDNA Transcription during Mitosis

As cells enter mitosis, nucleoli disassemble and Pol I transcription is shut down (Heix et al., 1998). FBL is released from rDNA, whereas SIRT7 and several components of the transcription machinery remain associated with NORs (Gébrane-Younès et al., 1997; Grob et al., 2009; Sirri et al., 2000). The topological separation of SIRT7 and FBL leads to hyperacetylation of FBL in mitotic cells (Figures 4A, 4B, and S4A). Mitotic hyperacetylation of FBL was not further augmented if SIRT7 activity was inhibited by NAM (Figure 4C). The H2AQ104me signal was lost in prometaphase, coinciding with hyperacetylation of FBL (Figure S4B). In control cells, the H2AQ104me mark was reestablished in early telophase, while in FBL- and SIRT7-depleted cells, H2AQ104me remained low (Figures 4D and S4C).

Significantly, cell-cycle-dependent changes of H2AQ104me correlated with fluctuations in pre-rRNA synthesis. Nucleolar transcription was shut down at prophase and was resumed at early telophase. After depletion of FBL or SIRT7, pre-rRNA synthesis did not recommence at telophase (Figure S4D), underscoring the requirement of both SIRT7 and FBL in reactivation of Pol I transcription at the exit from mitosis.

The impact of FBL deacetylation in the reestablishment of H2AQ104me and resumption of Pol I transcription at telophase was also shown by experiments monitoring the ability of ectopic FBL to restore H2AQ104me and rDNA transcription in FBL-depleted cells. Overexpression of wild-type FBL and 4KR-FBL restored H2AQ104me and nucleolar transcription, while overexpression of 4KQ-FBL promoted neither H2AQ104 methylation nor pre-rRNA synthesis in late telophase (Figures 4E and 4F). Together, these results demonstrate that hyperacetylation of FBL compromises H2AQ104 methylation and nucleolar transcription at the onset of mitosis. At the exit from mitosis, deacetylation of FBL by SIRT7 is required for deposition of H2AQ104me and transcription activation.

DISCUSSION

Previous work has established that SIRT7 is associated with rDNA and promotes cell growth and proliferation in response to external cues (Ford et al., 2006). SIRT7 deacetylates PAF53, a subunit of mammalian Pol I, which facilitates the association of Pol I with rDNA and augments transcription (Chen et al., 2013). Moreover, SIRT7 regulates processing of pre-rRNA by targeting and deacetylating U3-55k, which enhances its interaction with U3 snoRNA (Chen et al., 2016). The role of SIRT7 in ribosome biogenesis and cell proliferation has been highlighted by proteomic studies showing that SIRT7 is associated with numerous proteins with functions in transcription, ribosome biogenesis, and translation (Blank et al., 2017; Tsai et al., 2014). Among them was the nucleolar protein FBL (yeast Nop1), the enzyme that methylates both rRNA and nucleolar histone H2A. Given the importance of SIRT7 and FBL in ribosome biogenesis (Tollervey et al., 1991, 1993), we reasoned that SIRT7-dependent deacetylation of FBL might regulate 2′-*O*-methylation and pre-rRNA processing. Surprisingly, however, acetylation of FBL affected neither methylation nor processing of pre-rRNA. The RiboMeth-seq profiles in *SIRT7*$^{+/+}$ and *SIRT7*$^{-/-}$ cells were almost identical, indicating that FBL acetylation has no major impact on methylation of pre-rRNA.

We found that FBL acetylation regulates methylation of histone H2A at Q104, a specific epigenomic mark that is dedicated

(C) Acetylation of Fl-FBL from untreated (Ctrl) or NAM-treated (10 mM, 5 hr) asynchronous (AS) or mitotic (M) cells.
(D) Immunostaining of H2AQ104me (red) and UBF (green) in U2OS cells transfected with FBL- or SIRT7-targeting siRNAs and control siRNAs. DNA was counterstained with Hoechst 33342. Scale bar, 10 μm. See also Figure S4C.
(E) FBL-depleted U2OS cells expressing WT or mutant Fl-FBL were immunostained for H2AQ104me (red) and FBL (green). Hoechst 33342 staining of nuclei in late telophase is shown below. Scale bar, 10 μm.
(F) Cells transfected as in (E) were labeled with 5-FUrd for 10 min. Cells were stained with anti-BrdU (green) and anti-FBL (red). Hoechst 33342 staining of nuclei in late telophase is shown below. Scale bar, 10 μm.
Quantification in (E) and (F) shows mean intensity per nucleus (n = 30–40 telophase cells each from three biological replicates). Unpaired t test with Welch's correction was applied. ***$p \leq 0.001$.

to nucleolar transcription (Tessarz et al., 2014). In addition to acetylation (Choudhary et al., 2009; Schölz et al., 2015), FBL is post-translationally modified by ubiquitylation (Kim et al., 2011) and sumoylation (Hendriks et al., 2014). Replacement of four acetylated lysine residues by arginine or glutamine, which mimics the hypo- or hyperacetylated state of FBL, displayed different abilities to rescue H2AQ104me and pre-rRNA synthesis in FBL- or SIRT7-depleted cells. Thus, acetylation rather than other modifications of FBL impact H2AQ104me and Pol I transcription.

One could argue that reduced levels of H2AQ104me upon SIRT7 depletion are a consequence of decreased transcription. However, stimulation of Pol I transcription by overexpression of a constitutively active mutant of the Pol I transcription factor TIF-IA augmented neither FBL occupancy nor H2AQ104me levels, demonstrating that H2AQ104 methylation is not a consequence of enhanced transcription but requires deacetylation of FBL by SIRT7. While acetylation did not affect the interaction of FBL with pre-RNA, snoRNAs, or NOP58, acetylation abolished the interaction of FBL with histone H2A and impaired H2AQ104 methylation. Likewise, depletion of NOP58 attenuated H2AQ104me and pre-rRNA synthesis, indicating that FBL assembled into snoRNPs methylates H2AQ104.

The mechanism that governs H2AQ104me-dependent activation of Pol I transcription remains elusive. The region of H2A comprising Q104 has been shown to interact with FACT (facilitator of chromatin transcription), a conserved histone chaperone that destabilizes H2A/H2B dimers. FACT promotes transcription by disrupting nucleosomes and augmenting redeposition of nucleosomes in the wake of elongating RNA polymerase (Orphanides et al., 1998). Q104/5 resides in the "docking domain" at the nexus between H2A/H2B and H3/H4 dimers, where methylation may cause conformational changes reminiscent of that in H2A.Z, which contains a glycine at this position (Suto et al., 2000). In support of hypoacetylated FBL promoting H2AQ104 methylation and chromatin decompaction, our ChIP and FAIRE experiments show that depletion of FBL or SIRT7 leads to decreased rDNA occupancy of Pol I, low levels of acetylated histone H4, and chromatin compaction, indicating that H2AQ104 methylation establishes a transcription-permissive chromatin landscape. These results suggest that signaling pathways that induce SIRT7-dependent FBL hypoacetylation trigger H2AQ104 methylation and the establishment of a transcription-permissive chromatin structure.

The importance of SIRT7-dependent deacetylation of FBL on nucleolar transcription is most evident during cell-cycle progression. Transcription of rDNA oscillates during the cell cycle; it is maximal in S and G2 phases, repressed during mitosis, and gradually recovers during G1 progression (Klein and Grummt, 1999). Mitotic silencing of Pol I transcription is caused by Cdk1-cyclin-B-dependent phosphorylation of TAF_I110, leading to impaired assembly of the promoter selectivity factor SL1 and the Pol I transcription initiation complex (Heix et al., 1998). Dephosphorylation of SL1 at the end of mitosis relieves mitotic repression of Pol I transcription, indicating that phosphorylation of the Pol I-specific TBP-TAF complex is used as a molecular switch to shut off rDNA transcription during mitosis.

Here, we have uncovered an additional mechanism that regulates rRNA synthesis during cell-cycle progression. We show that the level of H2AQ104me is regulated by the dynamic interaction between SIRT7 and FBL. At the onset of mitosis, release of FBL to the chromosomal periphery is accompanied by hyperacetylation of FBL, loss of H2AQ104me and transcriptional shutdown. At the exit from mitosis, SIRT7-dependent deacetylation of FBL augments H2AQ104me and resumption of rRNA synthesis. The intriguing link between FBL acetylation and H2AQ104 methylation suggests that reversible acetylation regulates FBL-dependent H2AQ104me, which in turn facilitates efficient Pol I transcription.

STAR★METHODS

Detailed methods are provided in the online version of this paper and include the following:

- KEY RESOURCES TABLE
- CONTACT FOR REAGENT AND RESOURCE SHARING
- EXPERIMENTAL MODEL AND SUBJECT DETAILS
- METHOD DETAILS
  - Cell transfections and treatments
  - Expression and purification of recombinant proteins
  - *In vitro* deacetylation assay
  - Metabolic labeling of nascent RNA with 5-FUrd
  - Metabolic labeling of RNA with ^{3}H-uridine
  - Northern blotting
  - Crosslinked RNA immunoprecipitation (CLIP)
  - RiboMeth-seq
  - Immunofluorescence
  - Protein pull-down experiments and co-immunoprecipitation
  - Far-western blotting
  - Duolink Proximity Ligation assay (PLA)
  - Chromatin immunoprecipitation (ChIP)
  - Formaldehyde-assisted identification of regulatory elements (FAIRE)
  - Flow Cytometry
  - Histone extraction
- QUANTIFICATION AND STATISTICAL ANALYSIS
- DATA AND SOFTWARE AVAILABILITY

SUPPLEMENTAL INFORMATION

Supplemental Information includes four figures and two tables and can be found with this article online at https://doi.org/10.1016/j.celrep.2018.11.051.

ACKNOWLEDGMENTS

We thank Dr. Holger Bierhoff for discussions and critical reading of the manuscript, Dr. Renate Voit for initiating this work, and Bettina Dörr for technical assistance. Support by the German Cancer Research Center (DKFZ) Light Microscopy Facility is gratefully acknowledged. The work of I.G. was supported by the Helmholtz Foundation and by grants from the Deutsche Forschungsgemeinschaft (GR475/22-2 and SFB1036). The work of N.K. and H.N. was supported by grants from the Danish Research Council for Independent Research (DFF-4183-00486), the Lundbeck Foundation (R198-2015-174), and the Danish Cancer Society (R167-A10943-17-S2). Open access was funded by the DKFZ (Molecular Biology of the Cell II [A030]).

AUTHOR CONTRIBUTIONS

I.G. conceived and supervised the project. A.I.-B. designed and performed the experiments and analyzed the data. N.K. and H.N. performed RiboMeth-seq. P.T. provided the anti-H2AQ104me antibody and T.R. performed mass spectrometry. A.I.-B. and I.G. wrote the manuscript.

DECLARATION OF INTERESTS

The authors declare no competing interests.

Received: June 7, 2018
Revised: September 17, 2018
Accepted: November 12, 2018
Published: December 11, 2018

REFERENCES

Birkedal, U., Christensen-Dalsgaard, M., Krogh, N., Sabarinathan, R., Gorodkin, J., and Nielsen, H. (2015). Profiling of ribose methylations in RNA by high-throughput sequencing. Angew. Chem. Int. Ed. Engl. *54*, 451–455.

Blank, M.F., Chen, S., Poetz, F., Schnölzer, M., Voit, R., and Grummt, I. (2017). SIRT7-dependent deacetylation of CDK9 activates RNA polymerase II transcription. Nucleic Acids Res. *45*, 2675–2686.

Chen, S., Seiler, J., Santiago-Reichelt, M., Felbel, K., Grummt, I., and Voit, R. (2013). Repression of RNA polymerase I upon stress is caused by inhibition of RNA-dependent deacetylation of PAF53 by SIRT7. Mol. Cell *52*, 303–313.

Chen, S., Blank, M.F., Iyer, A., Huang, B., Wang, L., Grummt, I., and Voit, R. (2016). SIRT7-dependent deacetylation of the U3-55k protein controls pre-rRNA processing. Nat. Commun. *7*, 10734.

Choudhary, C., Kumar, C., Gnad, F., Nielsen, M.L., Rehman, M., Walther, T.C., Olsen, J.V., and Mann, M. (2009). Lysine acetylation targets protein complexes and co-regulates major cellular functions. Science *325*, 834–840.

Dundr, M., Misteli, T., and Olson, M.O.J. (2000). The dynamics of postmitotic reassembly of the nucleolus. J. Cell Biol. *150*, 433–446.

Ford, E., Voit, R., Liszt, G., Magin, C., Grummt, I., and Guarente, L. (2006). Mammalian Sir2 homolog SIRT7 is an activator of RNA polymerase I transcription. Genes Dev. *20*, 1075–1080.

Gébrane-Younès, J., Fomproix, N., and Hernandez-Verdun, D. (1997). When rDNA transcription is arrested during mitosis, UBF is still associated with non-condensed rDNA. J. Cell Sci. *110*, 2429–2440.

Grob, A., Roussel, P., Wright, J.E., McStay, B., Hernandez-Verdun, D., and Sirri, V. (2009). Involvement of SIRT7 in resumption of rDNA transcription at the exit from mitosis. J. Cell Sci. *122*, 489–498.

Heix, J., Vente, A., Voit, R., Budde, A., Michaelidis, T.M., and Grummt, I. (1998). Mitotic silencing of human rRNA synthesis: inactivation of the promoter selectivity factor SL1 by cdc2/cyclin B-mediated phosphorylation. EMBO J. *17*, 7373–7381.

Hendriks, I.A., D'Souza, R.C.J., Yang, B., Verlaan-de Vries, M., Mann, M., and Vertegaal, A.C.O. (2014). Uncovering global SUMOylation signaling networks in a site-specific manner. Nat. Struct. Mol. Biol. *21*, 927–936.

Kim, W., Bennett, E.J., Huttlin, E.L., Guo, A., Li, J., Possemato, A., Sowa, M.E., Rad, R., Rush, J., Comb, M.J., et al. (2011). Systematic and quantitative assessment of the ubiquitin-modified proteome. Mol. Cell *44*, 325–340.

Kiss-László, Z., Henry, Y., Bachellerie, J.P., Caizergues-Ferrer, M., and Kiss, T. (1996). Site-specific ribose methylation of preribosomal RNA: a novel function for small nucleolar RNAs. Cell *85*, 1077–1088.

Klein, J., and Grummt, I. (1999). Cell cycle-dependent regulation of RNA polymerase I transcription: the nucleolar transcription factor UBF is inactive in mitosis and early G1. Proc. Natl. Acad. Sci. USA *96*, 6096–6101.

Krogh, N., Jansson, M.D., Häfner, S.J., Tehler, D., Birkedal, U., Christensen-Dalsgaard, M., Lund, A.H., and Nielsen, H. (2016). Profiling of 2′-O-Me in human rRNA reveals a subset of fractionally modified positions and provides evidence for ribosome heterogeneity. Nucleic Acids Res. *44*, 7884–7895.

Loza-Muller, L., Rodríguez-Corona, U., Sobol, M., Rodríguez-Zapata, L.C., Hozak, P., and Castano, E. (2015). Fibrillarin methylates H2A in RNA polymerase I trans-active promoters in Brassica oleracea. Front. Plant Sci. *6*, 976.

Michishita, E., Park, J.Y., Burneskis, J.M., Barrett, J.C., and Horikawa, I. (2005). Evolutionarily conserved and nonconserved cellular localizations and functions of human SIRT proteins. Mol. Biol. Cell *16*, 4623–4635.

Orphanides, G., LeRoy, G., Chang, C.H., Luse, D.S., and Reinberg, D. (1998). FACT, a factor that facilitates transcript elongation through nucleosomes. Cell *92*, 105–116.

Schölz, C., Weinert, B.T., Wagner, S.A., Beli, P., Miyake, Y., Qi, J., Jensen, L.J., Streicher, W., McCarthy, A.R., Westwood, N.J., et al. (2015). Acetylation site specificities of lysine deacetylase inhibitors in human cells. Nat. Biotechnol. *33*, 415–423.

Sirri, V., Roussel, P., and Hernandez-Verdun, D. (2000). In vivo release of mitotic silencing of ribosomal gene transcription does not give rise to precursor ribosomal RNA processing. J. Cell Biol. *148*, 259–270.

Suto, R.K., Clarkson, M.J., Tremethick, D.J., and Luger, K. (2000). Crystal structure of a nucleosome core particle containing the variant histone H2A.Z. Nat. Struct. Biol. *7*, 1121–1124.

Tessarz, P., Santos-Rosa, H., Robson, S.C., Sylvestersen, K.B., Nelson, C.J., Nielsen, M.L., and Kouzarides, T. (2014). Glutamine methylation in histone H2A is an RNA-polymerase-I-dedicated modification. Nature *505*, 564–568.

Tollervey, D., Lehtonen, H., Carmo-Fonseca, M., and Hurt, E.C. (1991). The small nucleolar RNP protein NOP1 (fibrillarin) is required for pre-rRNA processing in yeast. EMBO J. *10*, 573–583.

Tollervey, D., Lehtonen, H., Jansen, R., Kern, H., and Hurt, E.C. (1993). Temperature-sensitive mutations demonstrate roles for yeast fibrillarin in pre-rRNA processing, pre-rRNA methylation, and ribosome assembly. Cell *72*, 443–457.

Tsai, Y.-C., Greco, T.M., and Cristea, I.M. (2014). Sirtuin 7 plays a role in ribosome biogenesis and protein synthesis. Mol. Cell. Proteomics *13*, 73–83.

Tyc, K., and Steitz, J.A. (1989). U3, U8 and U13 comprise a new class of mammalian snRNPs localized in the cell nucleolus. EMBO J. *8*, 3113–3119.

Voit, R., Hoffmann, M., and Grummt, I. (1999). Phosphorylation by G1-specific cdk-cyclin complexes activates the nucleolar transcription factor UBF. EMBO J. *18*, 1891–1899.

Zhao, J., Yuan, X., Frödin, M., and Grummt, I. (2003). ERK-dependent phosphorylation of the transcription initiation factor TIF-IA is required for RNA polymerase I transcription and cell growth. Mol. Cell *11*, 405–413.

STAR★METHODS

KEY RESOURCES TABLE

REAGENT or RESOURCE	SOURCE	IDENTIFIER
Antibodies		
Rabbit polyclonal anti-H2AQ104me (IF)	Tessarz et al., 2014	N/A
Rabbit polyclonal anti-UBF (ChIP)	Voit et al., 1999	N/A
Mouse monoclonal anti-UBF (IF)	Santa Cruz	Cat# sc-13125; RRID: AB_671403
Rabbit polyclonal anti-RPA116 (Pol I ChIP)	Voit et al., 1999	N/A
Rabbit polyclonal anti-SIRT7 (WB and IP)	Chen et al., 2016	N/A
Mouse monoclonal anti-FLAG (WB and IF)	Sigma-Aldrich	Cat# F3165; RRID: AB_259529
Rabbit polyclonal anti-GFP (WB)	Abcam	Cat# ab290; RRID: AB_303395
Mouse monoclonal anti-GFP (IF)	Abcam	Cat# ab1218; RRID: AB_298911
Monoclonal mouse anti-6X-His (WB)	Abcam	Cat# ab5000; RRID: AB_304722
Mouse monoclonal anti-BrdU (IF)	Sigma-Aldrich	Cat# B2531; RRID: AB_476793
Rabbit polyclonal anti-NOP58 (WB)	Atlas antibodies	Cat# HPA018472; RRID: AB_1854564
Rabbit polyclonal anti-histone H2A (WB)	Millipore	Cat# 07-146; RRID: AB_11212920
Rabbit polyclonal anti-histone H2A (PLA)	Abcam	Cat# ab88770; RRID: AB_10672053
Rabbit polyclonal anti-acetylated histone H4 (ChIP)	Millipore	Cat# 06-866; RRID: AB_310270
Rabbit polyclonal anti-histone H4 (ChIP)	Active Motif	Cat# 39269; RRID: AB_2636967
Rabbit polyclonal anti-histone H3 (WB)	Diagenode	Cat# C15310135
Rabbit polyclonal anti-acetyl-lysine (WB)	Cell signaling	Cat# 9441; RRID: AB_331805
Rabbit polyclonal anti-FBL (WB, IF and ChIP)	Abcam	Cat# ab5821; RRID: AB_2105785
Mouse monoclonal anti-FBL (IF and PLA)	Abcam	Cat# ab4566
Anti-rabbit HRP conjugate secondary antibody	Jackson ImmunoResearch Labs	Cat# 111-035-144; RRID: AB_2307391
Anti-mouse HRP conjugate secondary antibody	Jackson ImmunoResearch Labs	Cat# 115-035-062; RRID: AB_2338504
Goat anti-mouse Alexa Fluor 488 conjugate secondary antibody	ThermoFisher Scientific	Cat# A32723; RRID: AB_2633275
Goat anti-rabbit Cy3 conjugate secondary antibody	Jackson ImmunoResearch Labs	Cat# 111-165-144; RRID: AB_2338006
Bacterial and Virus Strains		
Baculovirus encoding human FLAG-SIRT7	Chen et al., 2013	N/A
Chemicals, Peptides, and Recombinant Proteins		
Nicotinamide (NAM)	Sigma-Aldrich	Cat# N3376
Trichostatin A (TSA)	Cell Signaling	Cat# 9950
Nicotinamide adenine dinucleotide (NAD^+), Lithium salt	Calbiochem	Cat# 481915
Nocodazole	Sigma-Aldrich	Cat# M1404
Hoechst 33342	Sigma-Aldrich	Cat# 14533
FLAG peptide	Sigma-Aldrich	Cat# F3290
His-tagged histone H1	Abcam	Cat# ab206452
His-tagged histone H2A	Abcam	Cat# ab200295
Protein A-HRP	ThermoFisher Scientific	Cat# 101023
Critical Commercial Assays		
TRI-Reagent	Sigma-Aldrich	Cat# T9424
M-MLV reverse transcriptase	ThermoFisher Scientific	Cat# 28025013
SuperScript IV reverse transcriptase	ThermoFisher Scientific	Cat# 18090010
Duolink Proximity ligation assay	Sigma-Aldrich	Cat# DUO92101
Muse Cell cycle assay kit	Merck Millipore	Cat# MCH100106
Lipofectamine 2000	ThermoFisher Scientific	Cat# 11668019
Lipofectamine 3000	ThermoFisher Scientific	Cat# L3000015

(*Continued on next page*)

Continued

REAGENT or RESOURCE	SOURCE	IDENTIFIER
Deposited Data		
RiboMeth-seq	NCBI Gene Expression Omnibus	GSE115360
Experimental Models: Cell Lines		
Human U2OS cell line	ATCC	HTB-96
Human HEK293T cell line	ATCC	CRL-11268
Oligonucleotides		
Primers used in qPCR, see Table S1	This study	N/A
Primers used for site-directed mutagenesis, see Table S1	This study	N/A
Northern blot probe, see Table S1	Chen et al., 2016	N/A
Non-targeting ON-TARGETplus SMARTpool siRNAs	Dharmacon	Cat# D-001810-10
hSIRT7 ON-TARGETplus SMARTpool siRNAs	Dharmacon	Cat# L-007774-01
hFBL ON-TARGETplus SMARTpool siRNAs	Dharmacon	Cat# L-011269-00
Silencer Select siRNAs against the 3′UTR of *FBL* mRNA	ThermoFisher Scientific	Cat# 4399665; (siRNA ID: s501803)
Silencer Select custom siRNAs against 3′UTR of *SIRT7* mRNA (Oligo 1)	ThermoFisher Scientific	Cat# 4399665; (siRNA ID: s523487)
Silencer Select custom siRNAs against 3′UTR of *SIRT7* mRNA (Oligo 2)	ThermoFisher Scientific	Cat# 4399665; (siRNA ID: s523488)
hNOP58 ON-TARGETplus siRNA	Dharmacon	Cat# J-017973-10
Recombinant DNA		
Plasmid: pEGFP-C1	Clontech	Cat# #6084-1
Plasmid: pCMV-Tag2a	Stratagene	Cat# 211172
Plasmid: pEGFP-C1-FBL	This study	N/A
Plasmid: pCMV-Tag2a-FLAG-FBL	This study	N/A
Plasmid: pEGFP-C1-SIRT7	Ford et al., 2006	N/A
Plasmid: pEGFP-C1-SIRT7-H187Y	Ford et al., 2006	N/A
Plasmid: p300-HA	Chen et al., 2013	N/A
Plasmid: HA-CBP	Chen et al., 2013	N/A
Plasmid: FLAG-PCAF	Chen et al., 2013	N/A
Plasmid: pFASTbac-FLAG-SIRT7	Chen et al., 2013	N/A
Plasmid: pcDNA-FLAG-TIF-IA-S649D	Zhao et al., 2003	N/A
Software and Algorithms		
CLUSTAL Omega		https://www.ebi.ac.uk/Tools/msa/clustalo
ImageJ		https://imagej.nih.gov/ij/
Other		
M2 anti-FLAG agarose resin	Sigma-Aldrich	Cat# A2220
GFP-Trap	Chromotek	Cat# gta-20

CONTACT FOR REAGENT AND RESOURCE SHARING

Further information and requests for reagents should be directed to and fulfilled by the Lead Contact, Dr. Ingrid Grummt (i.grummt@dkfz.de).

EXPERIMENTAL MODEL AND SUBJECT DETAILS

U2OS and HEK293T cells were purchased from ATCC (American Type Culture Collection) and grown in Dulbecco's modified Eagle's medium supplemented with 10% Fetal Bovine Serum (FBS) and 1% penicillin-streptomycin. Cells were maintained under standard growth conditions at 37°C and 5% CO_2 in a humidified atmosphere. HEK293T SIRT7 knockout cells (*SIRT7*$^{-/-}$) were generated by CRISPR/Cas9–mediated mutagenesis (Chen et al., 2016). HEK293T cells were transfected with lentiCRISPRv1 vectors harboring single guide RNAs (sgRNAs 1-4) which target different regions within exon 1 of *SIRT7*. Single clones were retrieved after 7 days

of puromycin selection (750 ng/mL), expanded and analyzed for SIRT7 expression by western blotting. Manifestation of the *SIRT7* mutations was verified by PCR and sequencing.

METHOD DETAILS

Cell transfections and treatments

HEK293T cells were transfected with precipitates of plasmid DNA and calcium phosphate, and U2OS cells with Lipofectamine 3000 (ThermoFisher Scientific) and harvested after 30 h. siRNAs were transfected with Lipofectamine 2000 (ThermoFisher Scientific) and cells were harvested after 48 h. For NOP58 knockdown, cells were transfected twice with siRNA and harvested after 96 h. HEK293T and U2OS cells were arrested by treatment with 100 ng/mL nocodazole for 16 h. Bright-field imaging revealed that 90% of HEK293T cells and 70%–80% of U2OS cells were arrested in mitosis. For immunofluorescence, U2OS cells were synchronized, fixed and immunostained as described in the immunofluorescence method section. For rescue experiments, cells were first transfected with siRNAs against the 3′UTR of *FBL* or *SIRT7* mRNA for 16-18 h followed by plasmid transfection and incubation for further 30 h. To inhibit KDACs and SIRT7, cells were treated for 5 h with 1 μM trichostatin A (TSA) or 10 mM nicotinamide (NAM), respectively.

Expression and purification of recombinant proteins

HEK293T cells expressing epitope-tagged proteins were lysed in buffer AM-300 (300 mM KCl, 20 mM Tris-HCl [pH 7.9], 5 mM $MgCl_2$, 0.2 mM EDTA, 10% glycerol, 0.5 mM DTT) supplemented with 0.1% NP-40, protease inhibitors (Roche protease inhibitor cocktail, 100 μM phenylmethylsulfonyl fluoride (PMSF), and KDAC inhibitors (1 μM TSA, 5 mM sodium butyrate, 10 mM NAM). Lysates were incubated at 4°C for 4 h or overnight with mouse or rabbit IgGs (Dianova) bound to protein A/G-Sepharose (GE Healthcare) or with M2 anti-FLAG beads (Sigma-Aldrich) or with GFP-Trap (ChromoTek). After washing in lysis buffer, tagged proteins were eluted by boiling in SDS sample buffer and analyzed on western blots. FLAG-tagged SIRT7 used in enzymatic assays was isolated from baculovirus-infected Sf21 cells. Baculovirus-infected Sf21 cells were harvested 48 h post-infection. Lysis and immunoprecipitation was carried out in AM-300/0.1% NP-40 buffer supplemented with protease inhibitors. FLAG-SIRT7 was eluted for 2 h at 4°C in AM-300/20% glycerol/0.1% NP-40 buffer containing 80 μg/mL FLAG-peptide (Sigma-Aldrich). Aliquots were flash-frozen in liquid nitrogen and stored at −80°C.

In vitro deacetylation assay

GFP-FBL co-expressed with HA-CBP in $SIRT7^{-/-}$ cells was immobilized on GFP-Trap (ChromoTek) in AM-300 buffer (300 mM KCl, 20 mM Tris-HCl [pH 7.9], 5 mM $MgCl_2$, 0.2 mM EDTA, 10% glycerol, 0.5 mM DTT) and incubated with FLAG-SIRT7 for 1 h at 30°C in 10 mM Tris-HCl [pH 8.0], 2 mM $MgCl_2$, 10% glycerol, 0.2 mM DTT, 2.5 mM NAD^+. Acetylation was monitored on western blots using anti-acetyl-lysine antibody.

Metabolic labeling of nascent RNA with 5-FUrd

U2OS cells grown on coverslips were labeled with 2 mM 5-fluorouridine (5-FUrd, Sigma-Aldrich) for 10 min, fixed with 1% paraformaldehyde for 10 min at room temperature, and permeabilized for 10 min on ice with 0.5% Triton X-100 in PBS. After blocking for 45 min with 3% BSA in PBS/0.2% Tween-20, the coverslips were incubated overnight at 4°C with anti-BrdU (1:1000) and anti-FBL (1:500) antibodies and stained with fluorophore-coupled secondary antibodies. DNA was stained with Hoechst 33342.

Metabolic labeling of RNA with ^{3}H-uridine

Cells were cultured for 3 h in medium containing 5 μCi ^{3}H-uridine (PerkinElmer). Cellular RNA (2 μg) was separated on denaturing 1% agarose gels in 20 mM MOPS, [pH 7.0], 5 mM sodium acetate, 1 mM EDTA. After transfer to Hybond-N+ nylon membranes (GE Healthcare), labeled RNA was visualized by fluorography using EN^{3}HANCE (PerkinElmer).

Northern blotting

Cellular RNA (3-5 μg) was separated on MOPS-agarose gels, transferred to Hybond N+ nylon membranes (GE Healthcare) and hybridized with ^{32}P-labeled ITS1 oligonucleotide (Table S1) for 16 h at 45°C in 6x SSC, 5x Denhardt's buffer, 0.5% SDS and 100 μg/mL yeast tRNA. After washing with 2x SSC/0.1% SDS and 1x SSC/0.1% SDS, radioactive signals were visualized by PhosphorImaging.

Crosslinked RNA immunoprecipitation (CLIP)

CLIP assays were performed as described (Chen et al., 2016). Briefly, nuclear lysates from UV-irradiated HEK293T cells (254 nm, 0.15 J/cm^2) were sonicated, precleared with protein G Sepharose (GE Healthcare), and protein-RNA complexes were immunoprecipitated using anti-FLAG M2 beads or protein G Sepharose coated with mouse IgGs. Beads were washed twice with IP buffer (20 mM Tris–HCl [pH 8.0], 200 mM NaCl, 1 mM EDTA, 1 mM EGTA, 0.1% SDS, 1% NP-40, 0.5% sodium deoxycholate, protease inhibitors) and twice with IP buffer containing 400 mM KCl. After elution with the FLAG peptide (80 μg/mL) and proteinase K digestion (30 min, 55°C), RNA was isolated, incubated with DNase I (Sigma-Aldrich), reverse transcribed using random hexamers (Roche) and MMLV reverse transcriptase (ThermoFisher Scientific), and subjected to RT-qPCR using primers listed in Table S1.

RiboMeth-seq

RiboMeth-seq analyses were performed according to a previously described protocol (Birkedal et al., 2015) in biological triplicates, except nuclear RNA from HEK293T *SIRT7*$^{-/-}$ cells, which was conducted in duplicates. In brief, cytoplasmic or nuclear RNA was degraded by alkaline hydrolysis into short fragments. The 20-40 nt fraction was excised and purified from gels. Sequencing adaptors were ligated to the fragments using a modified tRNA ligase and cDNA was synthesized using SuperScript IV reverse transcriptase (ThermoFisher Scientific). Libraries were sequenced on an Ion Proton sequencer, mapped against the rDNA reference sequence (Krogh et al., 2016), and scored for read-end counts. RiboMeth-seq scores (RMS) were calculated as previously described (''score C'' in (Birkedal et al., 2015) and presented as mean ± standard deviations (mean ± SD). In a few cases (indicated in Table S2), a barcode correction was applied when calculating the RMS. We have noted that commercially purchased RNA adaptors can be heterogeneous in length. If the 3′ adaptor is missing the first nucleotide at the 5′ end and then ligated to a library fragment with the identical nucleotide at its 3′ end, the nucleotide from the library fragment will be removed in the sequence processing step intended to trim off the adaptor sequence prior to mapping. Since libraries are made with different barcodes, such errors are easily detected and dealt with by excluding the 3′ read-end counts from the calculation at the affected site.

Immunofluorescence

U2OS cells grown on coverslips were fixed with 4% paraformaldehyde for 10 min at room temperature, permeabilized on ice for 10 min with 0.5% Triton X-100 in PBS. For H2AQ104me staining, CSK buffer (10 mM PIPES [pH 6.8], 100 mM NaCl, 300 mM sucrose, 3 mM $MgCl_2$, 1 mM EGTA, and 0.5% Triton X-100) was used. After blocking in PBS containing 3% BSA and 0.2% Tween-20 for 45 min, cells were incubated overnight at 4°C with the respective antibodies and stained with fluorophore-coupled secondary antibodies. Images were visualized with a Zeiss microscope (Axiophot) using a 40Å~1.3 oil immersion Plan-Neofluar magnifying objective, captured with a device camera (DS-Qi1Mc; Nikon) and processed with NIS-Elements software (version BR 3.10; Nikon). Images from at least three independent experiments were quantified using ImageJ software with at least 30-40 cells for each condition.

Protein pull-down experiments and co-immunoprecipitation

500 pmol of His-tagged histones H1 or H2A (purchased from Abcam) immobilized on 15 μL Ni-NTA agarose beads were incubated with precleared nuclear lysates for 4 h at 4°C in 50 mM NaH_2PO_4 [pH 7.9], 300 mM NaCl, 5 mM imidazole, 0.05% Tween-20 and protease inhibitors (Roche Complete, PMSF). After washing in binding buffer, bead-bound proteins were analyzed by western blotting. Uncoated Ni-NTA beads were used as background control. For pull-down assays, FLAG-tagged FBL or GFP-tagged SIRT7 were bound to M2-agarose or GFP-Trap in AM-buffer containing 150 mM KCl and proceeded as described in the protein purification section. Immunoprecipitation of endogenous SIRT7 was performed as described above with 3 μg homemade anti-SIRT7 antibodies (Chen et al., 2013). Immunoprecipitation with rabbit IgG served as negative control. Protein A-HRP (ThermoFischer Scientific) was used for detection to reduce IgG background as heavy chain IgG (~50 kDa) and endogenous SIRT7 (~45 kDa) migrate very close to each other.

Far-western blotting

FLAG-FBL was subjected to standard SDS-PAGE and transferred to a nitrocellulose membrane. The membrane was blocked at room temperature for 1 h in 5% skim milk in PBS/0.2% Tween-20. His-tagged histones H1 (ab206452) and H2A (ab200295) were diluted to a final concentration of 75 nM and incubated with filter-bound FLAG-FBL in binding buffer (100 mM NaCl, 20 mM Tris [pH 7.6], 0.5 mM EDTA, 10% glycerol, 0.1% Tween-20, 2% skim milk, 1 mM DTT) at 4°C for 16 h. After washing in PBS/0.2% Tween-20, anti-6X-His-tag (ab5000) antibody was used to detect bound histones and anti-FLAG antibody to monitor FLAG-FBL which migrates at 37 kDa.

Duolink Proximity Ligation assay (PLA)

The Duolink PLA assay was performed according to the manufacturer's instructions (Sigma-Aldrich). Briefly, U2OS cells were grown on coverslips, fixed with 4% paraformaldehyde for 10 min at room temperature and permeabilized in PBS containing 0.5% Triton X-100 for 15 min on ice. Cells were then blocked by incubation for 45 min in PBS with 3% BSA and 0.2% Tween-20 and incubated with primary antibodies (mouse anti-FBL and rabbit anti-H2A). After incubation with oligonucleotide-labeled secondary antibodies and ligation, DNA was amplified, hybridized to PLA probes and visualized by fluorescence microscopy.

Chromatin immunoprecipitation (ChIP)

Cells were fixed with 0.25% formaldehyde (10 min, room temperature) and quenched with 125 mM glycine for 5 min. Cells were lysed for 5 min in 5 mM HEPES [pH 8.0], 85 mM KCl and 0.5% NP-40. Nuclei were resuspended in 50 mM Tris-HCl [pH 8.1], 10 mM EDTA [pH 8.0], 1% SDS and sonicated with a Bioruptor UCD-200 (Diagenode) to yield 250–500 bp DNA fragments. After 5-fold dilution with 0.01% SDS, 1.1% Triton X-100, 1.2 mM EDTA, 16.7 mM Tris-HCl [pH 8.0], 167 mM NaCl and preclearing with protein A/G Sepharose, lysates were incubated overnight with the respective antibodies. Protein-DNA complexes were captured on protein A/G Sepharose (GE Healthcare) blocked with 0.05% BSA and 200 μg/μΛ *E. coli* DNA. In case of FLAG-tagged FBL ChIPs, M2 agarose beads were used to capture protein-DNA complexes overnight. Precipitates were washed in low salt buffer (150 mM NaCl, 50 mM Tris-HCl [pH 8.0], 5 mM $MgCl_2$, 1% Triton X-100), high salt buffer containing 500 mM NaCl, LiCl buffer (250 mM LiCl, 10 mM Tris-HCl

[pH 8.0], 5 mM EDTA, 0.5% Na-deoxycholate, 0.5% Triton X-100) and TE buffer. Immunoprecipitates were eluted in 50 mM $NaHCO_3$ solution containing 1% SDS. For FLAG ChIPs, immunoprecipitates were eluted for 4 h at 4°C in AM-300/10% glycerol/0.1% NP-40 buffer containing 80 μg/mL FLAG peptide (Sigma-Aldrich). After decrosslinking and proteinase K digestion, DNA was purified and analyzed by qPCR. Immunoprecipitated DNA was calculated as percentage of input DNA, after subtraction of background (IgG values). The primers used for qPCR are listed in Table S1.

Formaldehyde-assisted identification of regulatory elements (FAIRE)

Chromatin accessibility was monitored by FAIRE assay. Briefly, cells were crosslinked with 0.25% formaldehyde for 10 min at room temperature, quenched for 5 min with 125 mM glycine and lysed in FAIRE buffer 1 (50 mM HEPES-KOH [pH 7.5], 140 mM NaCl, 1 mM EDTA, 10% glycerol, 0.5% NP-40, 0.25% Triton X-100) at 4°C for 10 min. Nuclei were spun down (5,000 rpm, 5 min) and incubated in FAIRE buffer 2 (10 mM Tris-HCl [pH 8.0], 200 mM NaCl, 1 mM EDTA, 0.5 mM EGTA) for 10 min at room temperature. After an additional spin, sedimented chromatin was sheared in FAIRE buffer 3 (10 mM Tris-HCl, [pH 8.0], 100 mM NaCl, 1 mM EDTA, 0.5 mM EGTA, 0.1% sodium deoxycholate, 0.5% N-lauroylsarcosine) to an average length of 200-400 bp. Samples were cleared by centrifugation, 10% of the supernatants were removed as input and the rest was extracted twice with phenol/chloroform and once with chloroform. Input and extracted DNA were decrosslinked by incubation at 65°C for 16 h and purified with the QIAquick PCR purification kit (QIAGEN) followed by qPCR analysis.

Flow Cytometry

Approximately $1x10^6$ cells were fixed with ice-cold 70% ethanol and stored at −20°C for at least 3 h. Fixed cells were washed with PBS and stained with propidium iodide for 30 min in the presence of RNase A. Cells were analyzed on a MUSE flow cytometer (Merck) according to the manufacturer's protocol.

Histone extraction

HEK293T cells were harvested in PBS, washed, lysed in PBS containing 0.5% Triton X-100 and isolated nuclei were incubated in 0.2 N HCl at 4°C overnight. Extracts were cleared by centrifugation and neutralized with 0.1 volume of 1 M Tris base (Sigma-Aldrich). For western blotting, 2 μg of histones were loaded on 15% SDS polyacrylamide gels.

QUANTIFICATION AND STATISTICAL ANALYSIS

The values in the graphs show means of at least three independent experiments with error bars representing standard error of mean (SEM) unless otherwise specified. Data indicate representative immunofluorescence images of at least three independent experiments which were analyzed with at least 30-40 cells for each condition. In qPCR experiments, the two groups were compared using a paired two-tailed Student's t test. Column scatter-dot plots representing quantification of immunofluorescence images were drawn using Graphpad Prism. Unpaired two-tailed Student's t test with Welch's correction was used to calculate p values. The significance level was set at $*p \leq 0.05$ or $**p \leq 0.01$ or $***p \leq 0.001$. Ratio of FBL acetylation to FBL loading in western blots and H2A bound to immobilized FBL in Far-western experiments was quantified by densitometric analysis using ImageJ software. In each case the ratios were normalized to the control conditions (lane 1) within the given experiment. In the RiboMeth-seq analysis, error bars indicate standard deviation (SD) and significance was calculated using unpaired Student's t test for 2′-*O*-Me sites with a difference in mean RMS > 0.05. $*p \leq 0.05$, $**p \leq 0.01$.

DATA AND SOFTWARE AVAILABILITY

The accession number for the RiboMeth-seq data reported in this paper is NCBI Gene Expression Omnibus: GSE115360.